International Journal of Nanomedicine

Dovepress
open access to scientific and medical research

Open Access Full Text Article

ORIGINAL RESEARCH

Poly(Lysine)-Derived Carbon Quantum Dots Conquer *Enterococcus faecalis* Biofilm-Induced Persistent Endodontic Infections

Yongzhi Xu[1,2,*], Yuanping Hao[2,*], Muhammad Arif[3], Xiaodong Xing[4], Xuyang Deng[1], Danyang Wang[1], Yang Meng[2], Shuai Wang[1], Mohamed Sayed Hasanin[5], Wanchun Wang[2], Qihui Zhou[3,6]

[1]School of Stomatology, Qingdao University, Qingdao, People's Republic of China; [2]Department of Stomatology, Qingdao Stomatological Hospital Affiliated to Qingdao University, Qingdao, People's Republic of China; [3]Qingdao Key Laboratory of Materials for Tissue Repair and Rehabilitation, School of Rehabilitation Sciences and Engineering, University of Health and Rehabilitation Sciences, Qingdao, People's Republic of China; [4]School of Chemical Engineering, Nanjing University of Science and Technology, Nanjing, People's Republic of China; [5]Cellulose and Paper Department, National Research Centre, Dokki, Cairo, Egypt; [6]Hubei Key Laboratory of Biomass Fibers and Eco-Dyeing & Finishing, Wuhan Textile University, Wuhan, People's Republic of China

*These authors contributed equally to this work

Correspondence: Wanchun Wang; Qihui Zhou, Email kqwwch@126.com; qihuizhou@uor.edu.cn

Introduction: Persistent endodontic infections (PEIs) mediated by bacterial biofilm mainly cause persistent periapical inflammation, resulting in recurrent periapical abscesses and progressive bone destruction. However, conventional root canal disinfectants are highly damaging to the tooth and periodontal tissue and ineffective in treating persistent root canal infections. Antimicrobial materials that are biocompatible with apical tissues and can eliminate PEIs-associated bacteria are urgently needed.

Methods: Here, ε-poly (L-lysine) derived carbon quantum dots (PL-CQDs) are fabricated using pyrolysis to remove PEIs-associated bacterial biofilms.

Results: Due to their ultra-small size, high positive charge, and active reactive oxygen species (ROS) generation capacity, PL-CQDs exhibit highly effective antibacterial activity against *Enterococcus faecalis* (*E. faecalis*), which is greatly dependent on PL-CQDs concentrations. 100 μg/mL PL-CQDs could kill *E. faecalis* in 5 min. Importantly, PL-CQDs effectively achieved a reduction of biofilms in the isolated teeth model, disrupting the dense structure of biofilms. PL-CQDs have acceptable cytocompatibility and hemocompatibility in vitro and good biosafety in vivo.

Discussion: Thus, PL-CQDs provide a new strategy for treating *E. faecalis*-associated PEIs.

Keywords: carbon quantum dots, *Enterococcus faecalis*, bacterial biofilm, persistent endodontic infections

Introduction

Persistent endodontic infections (PEIs) mediated by bacterial biofilm mainly cause persistent periapical inflammation, resulting in recurrent periapical abscesses and progressive bone destruction. *Enterococcus faecalis* (*E. faecalis)* is the most frequently detected bacterium in reinfected root canals, especially in refractory periapical cases, with a detection rate of 24% to 77%.[1] The presence of persistent infection is the main cause of root canal treatment failure,[2] being the most common isolate.[3–7] They can adhere to the inner wall of the root canal, accumulate, and form organized biofilm communities, which contribute to its resistance to destruction, making the bacteria 1000 times[3] more resistant to phagocytosis, antibodies, and antimicrobial agents than organisms that do not produce biofilms. Traditional antimicrobial agents such as sodium hypochlorite (NaOCl), chlorhexidine (CHX), and calcium hydroxide are commonly used in endodontic treatment against microbial biofilms. However, their clinical use was limited by their inherent (bio)physicochemical properties. For instance, NaOCl is highly toxic to periapical tissue,[8] and the most common side effects of CHX as a mouthwash or topical oral gel are dry mouth (xerostomia), taste changes (loss of taste), a discolored or coated tongue,[9] contacting with calcium hydroxide for more than 7 days to play a good antibacterial

Received: 5 December 2023
Accepted: 18 May 2024
Published: 13 June 2024

Graphical Abstract

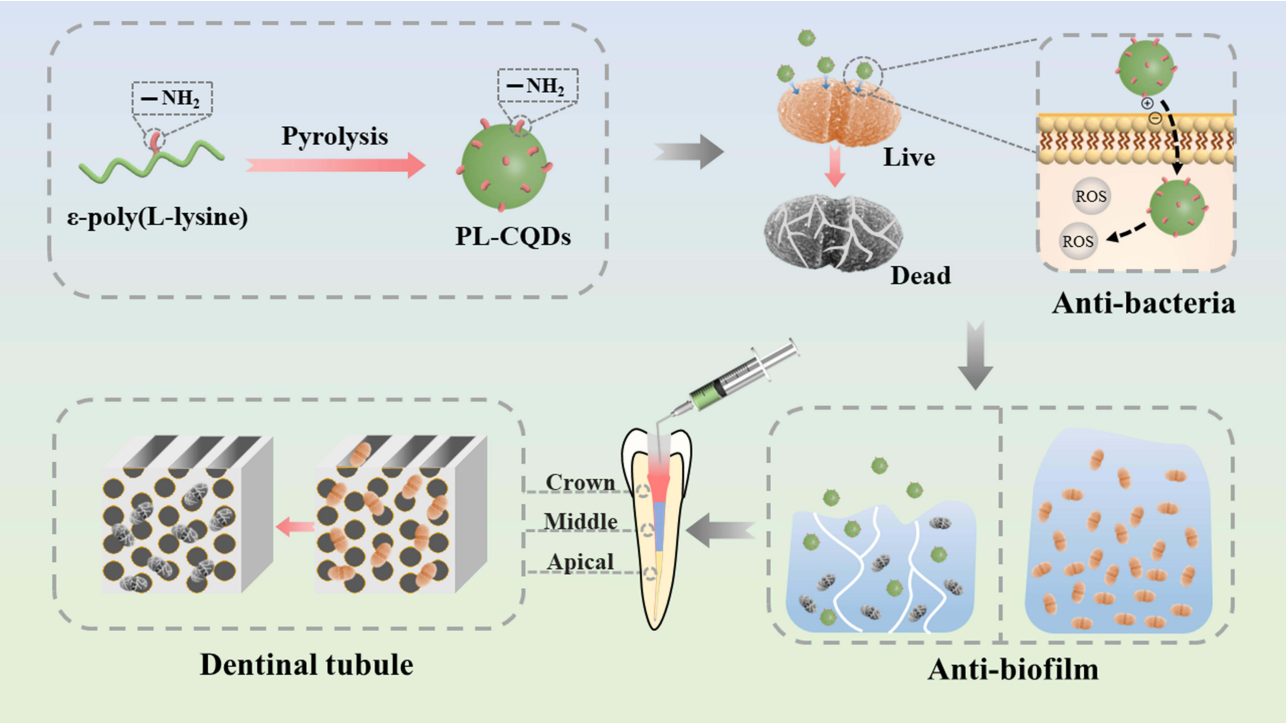

effect.[10,11] Therefore, it is necessary to develop new effective and non-toxic antimicrobial materials to eliminate persistent endodontic-associated bacterial/biofilm infections.

Nanoparticles, due to their ultra-small size (less than 100 nm in diameter), large surface area to mass ratio, high reactivity, and rich multifunctional integration, have been increasingly utilized in the biomedical field and are of great interest for their wide range of antimicrobial effects.[12–14] In endodontic studies, numerous nanoparticles with various components (eg, chitosan, zinc oxide, and silver) can disrupt biofilm structures and reduce bacteria in biofilms.[15,16] However, the size of these nanoparticles is still not small enough (~100 nm) and is likely to accumulate in the reticuloendothelial system with potential consequences.[17,18] The availability of carbon quantum dots (CDs) (1−10 nm) could compensate for the deficiencies above.

In the last few years, CDs have been widely used in nanomedicine,[19–21] bioimaging,[19–21] catalysis,[22] optoelectronics[23] and sensing[24] due to their desirable (bio)physicochemical and optical properties, including easy preparation, low toxicity, excellent photostability, good water dispersibility, and flexible surface functionalization,[25] while being considered as attractive bacterial inactivators. According to the available findings, the mechanisms of antimicrobial effects of CDs include the adhesion of CDs to bacterial surfaces, light-induced production of ROS, disruption and penetration of bacterial cell walls/membranes, induction of oxidative stress and damage to DNA/RNA, leading to altered or suppressed expression of important genes, and induction of oxidative damage to proteins and other intracellular biomolecules.[26–28] There have been numerous studies demonstrating the excellent bactericidal effect of carbon dots against various antimicrobial agents, such as *Bacillus subtilis*,[29–31] *Staphylococcus aureus*,[31–36] *Escherichia coli*,[30,31,33,35,37–42] *Klebsiella pneumoniae*,[36] *Methicillin-resistant Staphylococcus aureus*.[31,39] However, articles on carbon dots against *E. faecalis* and applied to treatment of PEIs have not been examined.

Inspired by the above presentation, we hypothesize that carbon dots as root canal disinfectants could treat persistent root canal infections with desirable bactericidal effects. In this work, we applied ε-poly (L-lysine) carbon quantum dots (PL-CQDs) aqueous solution as a potential root canal flushing agent to study its inhibitory effect on planktonic

E. faecalis and their biofilms and performed flushing tests on isolated teeth. In addition, the in vitro hemocompatibility/cytocompatibility and in vivo biosafety of PL-CQDs were tested.

Experimental Section

Materials

ε-poly (L-lysine) (PL) (MW~ 4000) purchased from Dipper Chemical Technology Co. (Shanghai, China). Dialysis membrane (MWCO = 5000 Da) supplied by Yanshun Biotechnology Co. (Qingdao, China). Brain Heart Infusion (BHI), Agar, ROS Assay Kit, and PBS (phosphate buffered solution) were purchased from Solarbio Science & Technology Co., Ltd. (Beijing, China). LIVE/DEAD Biofilm Viability Kit supplied by Thermo Fisher Scientific Inc. (Waltham, MA, USA). Dulbecco's modified Eagle's medium (DMEM), fetal bovine serum (FBS), penicillin, and streptomycin were obtained from Biological Industries Co., Ltd. (Beit-Haemek, Israel). The Cell Counting Kit-8 (CCK-8) was provided by MedChem Express Co., Ltd (Shanghai, China). All reagents were used directly without further purification.

Preparation of PL-CQDs

PL-CQDs were synthesized using a pyrolytic procedure. Briefly, 1 g PL powder was placed on a corundum crucible and heated in a box muffle oven at 240°C for 3 h. After the furnace cooled naturally to room temperature, the residue was ground into powder and dissolved in 20 mL of deionized water. The mixture was then sonicated for 60 min, centrifuged (11,000 rad/min) for 30 min, followed by dialysis of the supernatant with deionized water for 24 h and lyophilized (Alpha1-2 LD plus; CHRIST®, Germany). PL-CQDs powder was stored at 4°C.

Physicochemical Characterization

The morphology and size of PL-CQDs were examined using high-resolution transmission electron microscopy (HRTEM, JEM-2100F, Japan). The size distribution was determined from TEM images using ImageJ software.

X-ray photoelectron spectroscopy (XPS) was performed by an X-ray photoelectron spectrometer PHI5000 Versaprobe III ultrahigh vacuum (1×10^{-9} bar) unit with an Al Kα X-ray source and a monochromator. The X-ray beam size was 100 μm, measured spectra were recorded bypass energy (PE) 280 eV, and high energy resolution spectra were recorded with PE 112 eV. The XPS results were processed using the AVANTGE program.

The PL and PL-CQDs were dispersed in deionized water at the same concentration, and their Zeta potential (Z) was obtained using dynamic light scattering (DLS) at 25°C using the instrument Zeta sizer (Nano ZSE, UK).

Ultraviolet-visible spectrophotometry (UV–Vis) absorption spectra were detected using a Yuanxi UV-8000 spectrometer (Shanghai, China). The fluorescence spectra were characterized by a fluorescence (FL) spectrophotometer (MAPLETTA UV-6300, UK).

Bacterial Experiments

A single colony of *E. faecalis* (*E. faecalis* standard strain ATCC29212, Comprehensive Dental Care, Faculty of Dentistry, University of Hong Kong, Hong Kong, China) was suspended in 5 mL of BHI broth and grown overnight at 37°C. *E. faecalis* was harvested at the exponential growth phase via centrifugation. Colony-forming units (CFU) were used to calculate the concentration of bacteria, which was 1.0×10^7 CFU/mL, standardized by comparison with the 0.5 McFarland standard. Next, 1mL of PL-CQDs solution was added into the bacteria suspensions (1.0×10^7 CFU/mL, 1mL) with different final PL-CQDs concentrations (0, 25, 50, and 100 μg/mL) and incubation at 37°C for 5, 10 and 15 min, respectively. 2% CHX (chlorhexidine) was used as the positive control group. Subsequently, 20 μL of bacteria solutions were spread onto the BHI agar plates and incubated for 24 h at 37°C. The experiment was repeated thrice for each group.

ROS Assay

The ROS assay kit was used to measure intracellular ROS levels. A single colony of *E. faecalis* was incubated at 37°C for 18 h. After that, the obtained bacterial solution was mixed with an equal volume of different concentrations of PL-CQDs solution, incubated for 1 min, and centrifuged. Subsequently, the precipitate was resuspended with 1 mL of DCFH-DA and incubated at

37°C for 20 min. After washing the medium 3 times, resuspend the bacterial solution with 400 μL of PBS. The fluorescence intensity was measured at 488 nm excitation wavelength and 525 nm emission wavelength using a microplate reader. Each group's remaining 1 mL of liquid was used for bacteria counting. The experiment was repeated three times independently.

Scanning Electron Microscopy (SEM) Images of Bacteria

1 mL of 10^9 CFU/mL suspension of *E. faecalis* was mixed with 1 mL of PBS solution of PL-CQDs at a 1 mg/mL concentration for 2 min. The liquid medium was then removed by centrifugation at 5000 rpm for 5 min. The bacterial cells were washed thrice with PBS (pH 7.4) and then fixed with 2.5% glutaraldehyde for 24 h. Then, samples were dehydrated with 30%, 50%, 70%, 80%, 90%, 95% and 100% ethanol solutions. The samples were dried with a critical point drier, and the morphology of the bacteria was observed by SEM (VEGA3, TESCAN, Czech) after gold spraying.

Anti-Biofilm Experiment

Biofilm Culture

Using the continuous culture method, 1 mL of *E. faecalis* suspension (10^8 CFU/mL) was dispensed on glass coverslips in a sterile 24-well microtiter plate anaerobically at 37°C. 1 mL of fresh sterile BHI broth was replaced every other day for a 28 d incubation.

Anti-E. faecalis Biofilms

Carefully remove the medium and rinse 3 times with PBS to remove the planktonic bacteria. Different concentrations of PL-CQDs (1 mL) were added to each well. PBS and 2% CHX were used as the negative and positive control groups. After co-incubation for 24 h, biofilms were treated with a LIVE/DEAD Biofilm Viability Kit containing SYTO 9 and propidium iodide (PI) for 15 min at room temperature in the dark to label the live and dead bacteria. After being strained, bacteria with an intact membrane present green fluorescence, and the bacteria with an impaired membrane structure mainly show red fluorescence when observed by a confocal laser scanning microscope (CLSM). A Leica TCSSP8 CLSM (Leica Microsystems, Germany) was employed to image the stained biofilms. The experiment was repeated three times with three independent replications.

Anti-Biofilm Experiment on Isolated Teeth

Preparation of Isolated Teeth

Single-rooted healthy mandibular first premolars (n = 20) were collected from patients aged 13–18 for orthodontic reasons. After the root canal was evacuated with a 15# K-file, the Protaper nickel-titanium system was used to prepare the root canal to F2 using a crown-down approach. EDTA gel was applied during root canal preparation to remove the stained layer, while 1% sodium hypochlorite solution and saline were rinsed alternately. Finally, the root canal was ultrasonically cleaned for 1 min.

Biofilm Cultured in Isolated Teeth

The prepared teeth were sterilized at 121°C and placed in 5 mL Eppendorf (EP) tubes to ensure that the teeth were upright. After adding 1 mL of BHI broth to each tube, the mixture was left to incubate for 48 h at 37°C in a temperature-controlled environment. In the same manner as the biofilm produced on glass slides, 1 mL of E. faecalis suspension (108 CFU/mL) was added, and the mixture was incubated for 28 days at a consistent temperature of 37°C. The BHI broth was replaced every 2 d.

Anti-E. faecalis Biofilms in Isolated Teeth

After co-incubation, the morphologies of biofilm treated with PL-CQDs (100 and 1000 μg/mL), PBS, and 2% CHX were characterized by SEM. Briefly, the treated biofilms on the isolated teeth were carefully rinsed three times with PBS and fixed in 2.5 wt% glutaraldehyde for 1 h at 25°C. The fixed samples were dehydrated in an ethanol series (30, 40, 50, 70, 80, and 90%), each for 10 min, then in 100% ethanol for 15 min twice, and finally dried in a vacuum oven for 24 h. The specimens were observed by SEM operated at an acceleration voltage of 10 kV after being coated with gold.

Hemolysis Assay

Take 1 mL of anticoagulated blood from healthy rats and dilute it with 0.9% saline (5 mL). Then, the diluted blood solution (50 μL) was added into EP tubes containing different concentrations of PL-CQDs solution (1 mL), ultrapure water (positive control), and 0.9% saline (negative control), respectively. The mixture was incubated at 37°C for 1 h, centrifuged at 5000 rpm for 5 min, and the absorbance of the supernatant at 540 nm was measured using a microplate reader (PowerWave X, BioTek). The experiment was performed in triplicate. The hemolysis rate (hemolysis%) is calculated as follows:

$$\text{Hemolysis\%} = \frac{\text{Abs} - \text{Abs}(-)}{\text{Abs}(+) - \text{Abs}(-)} \times 100\%$$

In vitro Cytotoxicity Evaluation

Cell Culture

A mouse fibroblast cell line (L929) was obtained from the Cell Culture Center, Shanghai Institute of Life Sciences, Chinese Academy of Sciences, (Shanghai, China). L929 cells were cultured and expanded in the basal medium of DMEM containing 10% FBS and 1% penicillin/streptomycin at 37°C with 5% CO_2.

Cytotoxicity Assay

Cell viability assays were performed using CCK-8. Briefly, L929 cells were added to 96-well plates at a density of approximately 5000 cells/well and incubated with 100 μL of medium for 24 h. Subsequently, 100 μL of PL-CQDs solution with different concentrations was added to the plates and incubated for 24, 48, and 72 h. The PL-CQDs solution was replaced with 100 μL of new medium spiked with 10 μL of CCK-8 solution, and the absorbance at 450 nm was measured after 1 h of incubation. The viability of L929 was calculated using the following formula:

$$\text{Relative viability}\,(\%) = \frac{\text{OD}_{\text{Test450}}}{\text{OD}_{\text{Control450}}} \times 100\%$$

The experiment was performed in triplicate.

In vivo Biosafety Evaluation

Animal experiments followed the ARRIVE guidelines and be carried out in accordance with the UK Animals (Scientific Procedures) Act, 1986 and associated guidelines, EU Directive 2010/63/EU for animal experiments. All animals were treated humanely during the whole experiment. Adult SD rats (half male and half female, 10 weeks old, 200 g) were randomly divided into 2 groups and instilled with 5 mL of PL-CQDs saline solution (1 mg/mL) and 0.9% NS, respectively. By intraperitoneal injection of 10% chloral hydrate on the third and seventh day, 3 mL of blood was taken from the apex of the heart for routine blood and liver and kidney function tests. The rats' hearts, liver, spleen, lungs, and kidneys were collected and stored in 10% formalin to prepare pathological slides. After being stained with H&E, histological images were obtained on an optical microscope (Nikon, Japan).

Statistical Analysis

All the data were presented as mean values ± standard deviation based on experiments performed in triplicate. The statistical analysis was performed with GraphPad PRISM 8.0. Statistical significance was determined using one-way analysis of variance (ANOVA), and the significant differences in the data are shown with * $p < 0.05$, ** $p < 0.01$, and *** $p < 0.001$.

Results and Discussion

Preparation and Characterization of PL-CQDs

Smaller particle size CDs were reported to cross the lipid bilayer more efficiently and exhibit superior antimicrobial activity.[43–45] TEM images display the quasi-spherical morphology of the PL-CQDs with homogeneous size dispersion. The average particle size of PL-CQDs was 2.3 ± 0.36 nm (Figure S1). The smaller size makes it easier for PL-CQDs to

cross the lipid bilayer and interact with DNA molecules. Also, the HRTEM image reveals the crystalline nature of PL-CQDs with the lattice spacing of 0.21 nm, corresponding to the (100) facet of graphitic,[46] which suggests a stable crystal structure. (Figure 1A).

As shown in Figure 1B, the UV–Vis absorption spectrum of PL-CQDs displayed a strong absorption peak at 280 nm and a broad band from 300 to 400 nm, which are attributed to the π–π* transition of C = C and C – C as well as n–π* transition of C – O, C = O and C – N bonds, respectively. The macroscopic photographs of well-dispersed PL-CQDs under sunlight and 365 nm UV light showed pale yellow and blue in the inset of Figure 1B, respectively. Further, PL-CQDs were characterized by XPS to elucidate the elemental compositions. As shown in Figure S2A, there were distinguishing peaks for the carbon, nitrogen, and oxygen elements in PL-CQDs, with atomic concentrations of 74.80, 16.16, and 9.04%, respectively. The deconvoluted C 1s spectrum of PL-CQDs (Figure 1C) revealed three types of carbon bonds: C–C corresponding to sp3 (284.8 eV, 67.25%), C–N (286.1 eV, 23.44%), and O–C=O (287.89 eV, 9.31%). The O 1s spectrum (Figure S2B) showed two types of oxygen bonds, O–C (531.6 eV, 91.45%) and O=C (533.07 eV, 8.55%). The N 1s spectrum (Figure 1D) indicated two types of nitrogen bonds, –NH (399.74 eV, 66.32%) and $–NH_2$ (400.96 eV, 33.68%). The results confirmed the presence of primary amines on the surface of PL-CQDs, which is related to the charge of PL-CQDs. As expected, the PL-CQDs exhibited the charge property of the precursor PL (27.67 ± 4.12 mV) (Figure 1E). The high charge density could enhance the electrostatic interaction of PL-CQDs with negatively charged cell membranes and the ability to bind to intracellular negatively charged materials such as DNA and RNA.[47] Furthermore,

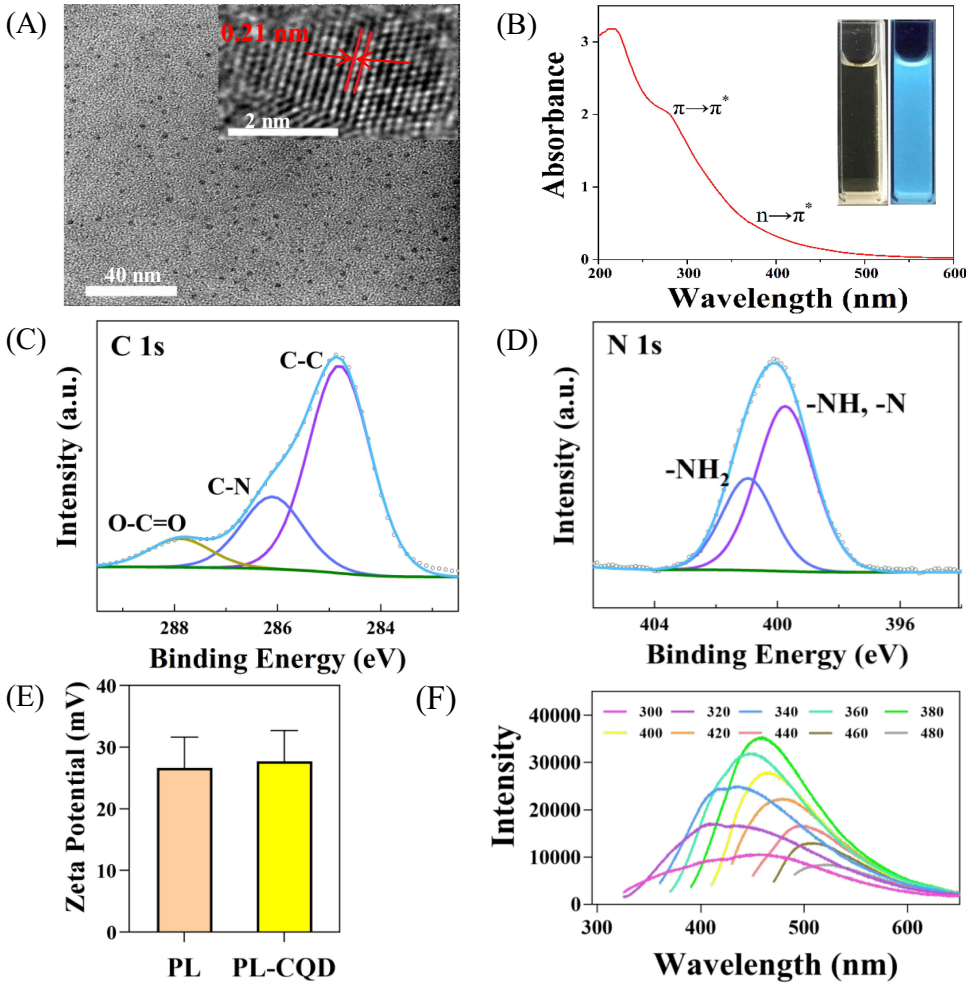

Figure 1 (**A**) TEM and HRTEM images of PL-CQDs. (**B**) UV–Vis absorption spectrum of PL-CQDs. The inserted part was photographs of PL-CQDs aqueous solution in sunlight and UV light. (**C**) XPS C 1s spectra of PL-CQDs. (**D**) XPS N 1s spectra of PL-CQDs. (**E**) Zeta potentials of PL and PL-CQDs. (**F**) Photoluminescence spectra of PL-CQDs.

the photoluminescence of PL-CQDs (Figure 1F) depended on the excitation wavelength, with the highest intensity emitted by PL-CQDs dispersions at 480 nm under excitation at 380 nm. When the excitation wavelength was increased from 300 to 480 nm, a significant red shift was observed in the emission.

Antibacterial Activity and ROS Generation of PL-CQDs

Based on the routine single tube preparation time in clinical practice, PL-CQDs co-cultured with *E. faecalis* for 5, 10, and 15 min. As shown in Figure 2A, no *E. faecalis* colonies existed on the plate with the PL-CQDs groups (ie, 25 μg/mL + 15 min, 50 μg/mL + 10 min, and 100 μg/mL + 5 min) and 2% CHX positive control group. The quantitative results in Figure 2B further indicate that the bactericidal effect of PL-CQDs showed a concentration and time dependence.

It is known that CQDs have large edge effects and quantum confinement, which result in unique electron transport properties.[48] The so-formed electron-hole pairs can react with surrounding molecular oxygen or water to form various types of ROS. ROS levels were measured using a ROS detection kit to verify whether the inhibitory activity against *E. faecalis* is related to the release of ROS. It was found that the intracellular fluorescence intensity of *E. faecalis* increased significantly upon exposure to PL-CQDs, and a large amount of ROS was produced within a short period of 1 min. Also, the higher the concentration of PL-CQDs (100 μg/mL), the stronger the fluorescence intensity (Figure 2C), which was positively correlated with the antibacterial effect (Figure S3).

To further explore the antibacterial mechanism of PL-CQDs, SEM images of the bacteria were obtained. As shown in Figure 2D, the morphology of the untreated bacteria was compact and retained the smooth surface feature; however, after the treatment with PL-CQDs for 2 min, the bacterial membrane shows multiple irregular ruptures, the cytosol flowed out, swollen and enlarged (Figure 2E). This multi-point cell destruction may be related to the positive charge nature of PL-CQDs, which has the advantage of a non-selective physical charge-charge interaction mechanism and does not induce bacterial resistance.[49]

The possible antibacterial mechanism of PL-CQDs was attributed to the tiny size, and the positive charge allows multiple points of rapid entry into the bacteria. At the same time, ROS produced by the PL-CQDs damages the bacteria's proteins, lipids, metabolites, and nucleotides. The rapid loss of intracellular fluid changes the bacteria's internal environment, causing immediate death (Figure 2F).

Anti-Biofilm Evaluation of PL-CQDs

The bacterial biofilm in the root canal induced by environmental factors could release some planktonic bacteria, causing acute episodes of chronic infection. The planktonic bacteria could wander to other surrounding sites, re-adhere, and reproduce to form new biofilms, leading to persistent root canal infection and periapical inflammation.[50,51] Encouraged by the antimicrobial advantages of PL-CQDs above, their antibiofilm performance was evaluated. *E. faecalis* biofilms were obtained through incubation on glass slides for 4 weeks.[52] After co-culturing with different concentrations of PL-CQDs, Live/Dead staining was performed to evaluate their antibiofilm ability. The corresponding fluorescent images of biofilm using 3D CLSM are shown in Figure 3. The biofilm in the control group was very uniform and dense. As a positive control group, 2% CHX had a certain biofilm killing effect, but relatively strong green fluorescence still was observed. Notably, in the study, PL-CQDs with a concentration of 100 μg/mL did not have a significant killing effect on the E. faecalis biofilm, which may be due to the extracellular polymeric substance (EPS) of the biofilm with an effective protective mechanism. With this concentration of PL-CQDs, the structure of the *E. faecalis* biofilm showed a marked transformation: it was efficiently broken down into isolated island structures composed of bacterial clusters. This remarkable change implies that PL-CQDs were able to destroy *E. faecalis* biofilm via adhering to the bacteria well, penetrating EPS, transforming into a free state. When the concentration of PL-CQDs was further increased to 1000 μg/mL, this destructive effect was significantly enhanced, the integrity of the *E. faecalis* biofilm was greatly damaged, and the biofilm could not continue to maintain the adhesion state on the surface of the glass. The analysis of CLSM cross-sectional images showed that the biofilm showed green fluorescence at a concentration of 100 μg/mL and the biofilm showed red fluorescence in the upper layer covered by green fluorescence in the bottom layer at a concentration of 500 μg/mL. When the concentration of PL-CQDs was increased to 1000 μg/mL, red fluorescence in the whole layer was observed, which indicated that the PL-CQDs within biofilm penetration and bactericidal effect is a layer-by-layer process dependent on PL-CQD concentrations. The mechanism of biofilm destruction was due to the synergistic effect of the ultrasmall size of PL-CQDs, its positive surface charge, and the generated reactive oxygen species. In the 2% CHX-treated group, there was a significant thickness of green fluorescence present in

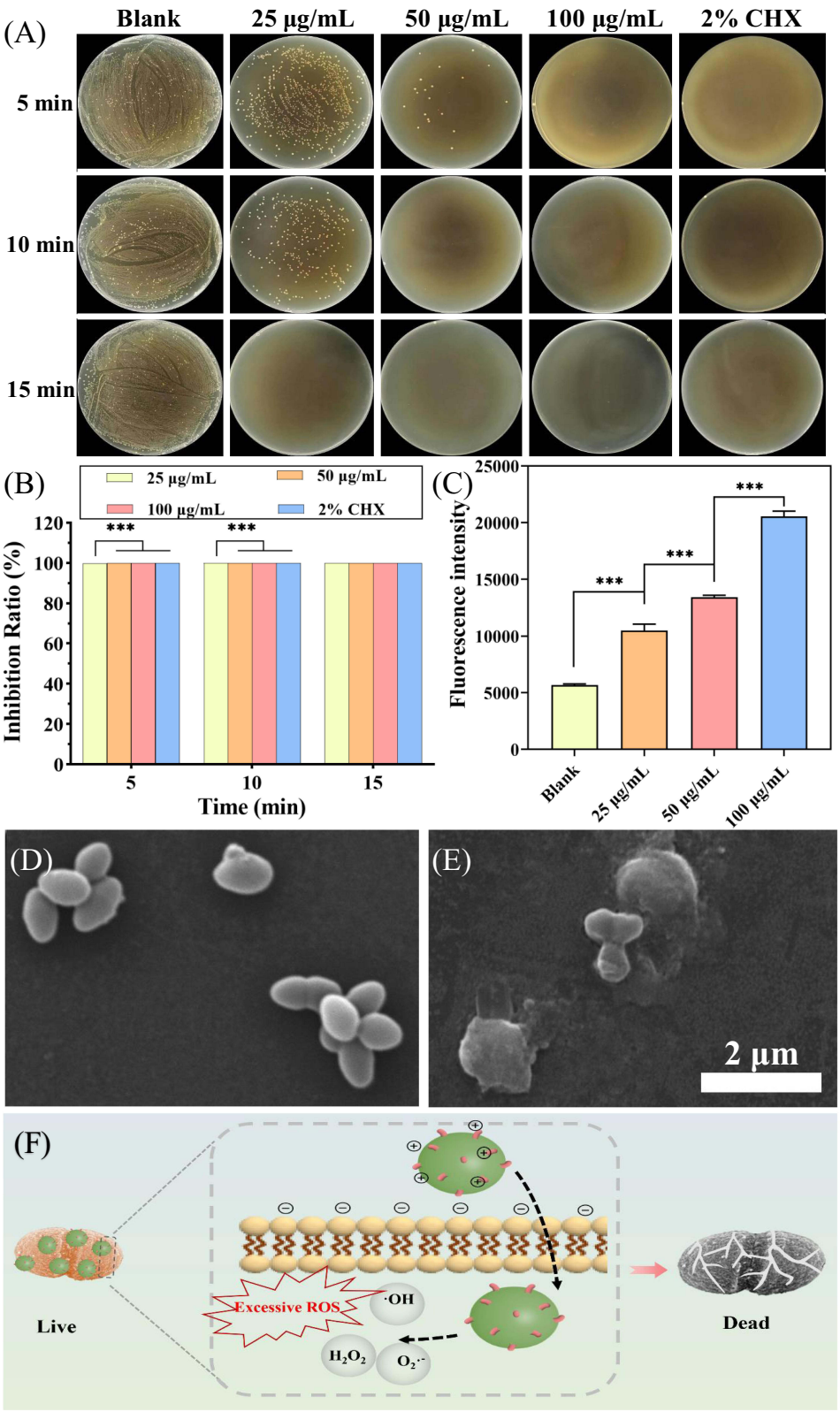

Figure 2 (**A**) Photographs of survival bacteria colonies of *E. faecalis* on agar plates after treatment with corresponding concentrations of PL-CQDs at different times. (**B**) The calculated inhibition ratio of *E. faecalis*. ***p< 0.001. (**C**) The intracellular ROS contents of *E. faecalis* in cells after PL-CQDs treatment. SEM images of (**D**) bacteria untreated with PL-CQDs and (**E**) treated with PL-CQDs. (**F**) Schematic diagram of the interaction between PL-CQDs and bacteria.

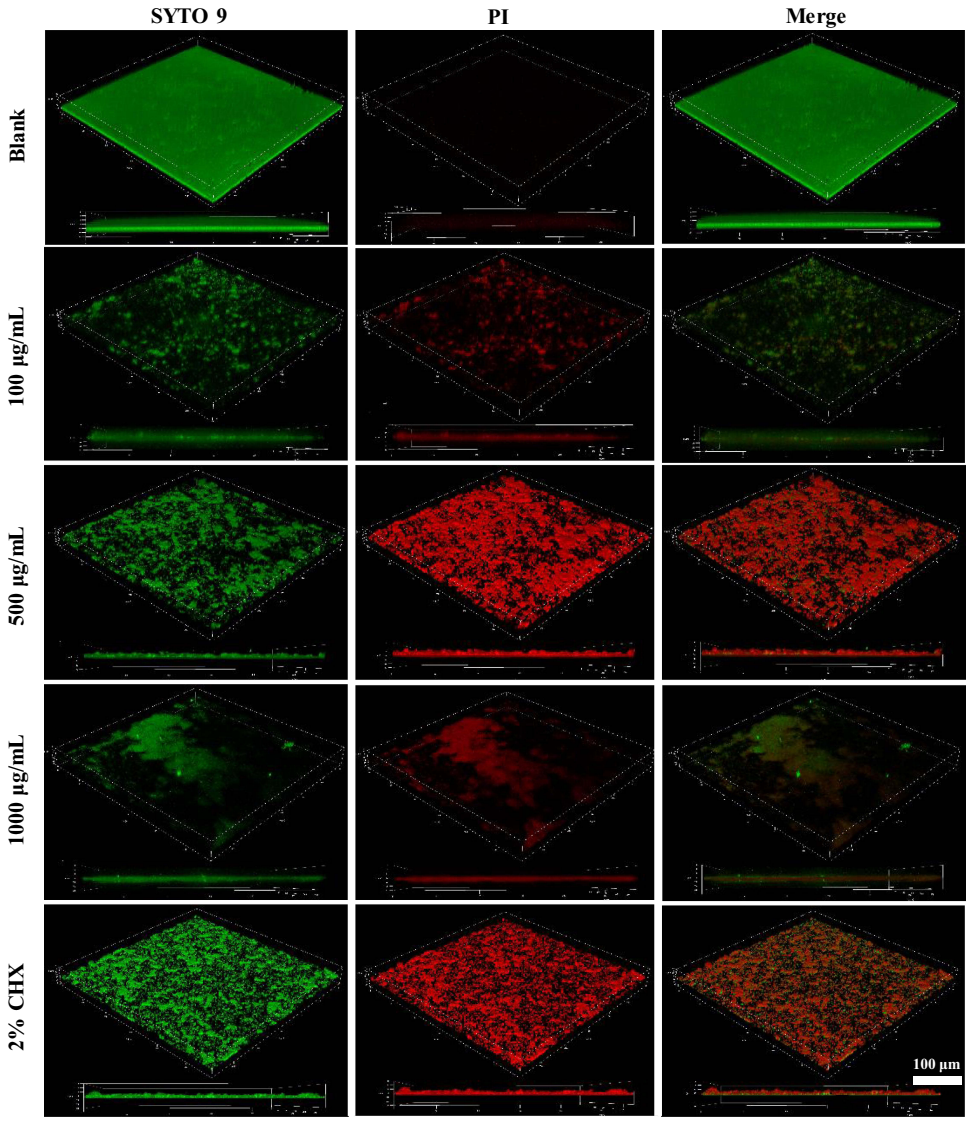

Figure 3 3D-CLSM images of *E. faecalis* biofilm inhibition on the glass slides. Green (SYTO 9) and red (PI) represent the live and dead cells of *E. faecalis*.

the bottom layer of the biofilm, indicating that its penetration and bactericidal efficiency on the biofilm was not as good as that of the 500 μg/mL PL-CQDs-treated group. This finding demonstrates the potential of PL-CQDs to be applied as root canal disinfectants beyond conventional disinfectants, showing excellent biofilm disruption and antimicrobial properties.

Anti-Biofilm Evaluation on the Isolated Teeth

The anti-biofilm ability of PL-CQDs was further evaluated using the isolated teeth model. SEM observation was conducted to assess qualitatively the elimination effect of biofilm in different parts of the root (crown 1/3, middle 1/3, and apical 1/3) treated with PL-CQDs (Figure 4). It was found that the biofilm with a certain thickness was formed on the inner wall of the dentin of the control group. The bacteria were distributed in clusters or chains. However, the number of bacteria on the inner wall of the root canal decreased significantly with the addition of PL-CQDs. The anti-biofilm effect showed a concentration dependence. 1000 μg/mL of PL-CQDs had an anti-biofilm similar impact with a 2% CHX group in the crown, middle, and apical 1/3 of the root.

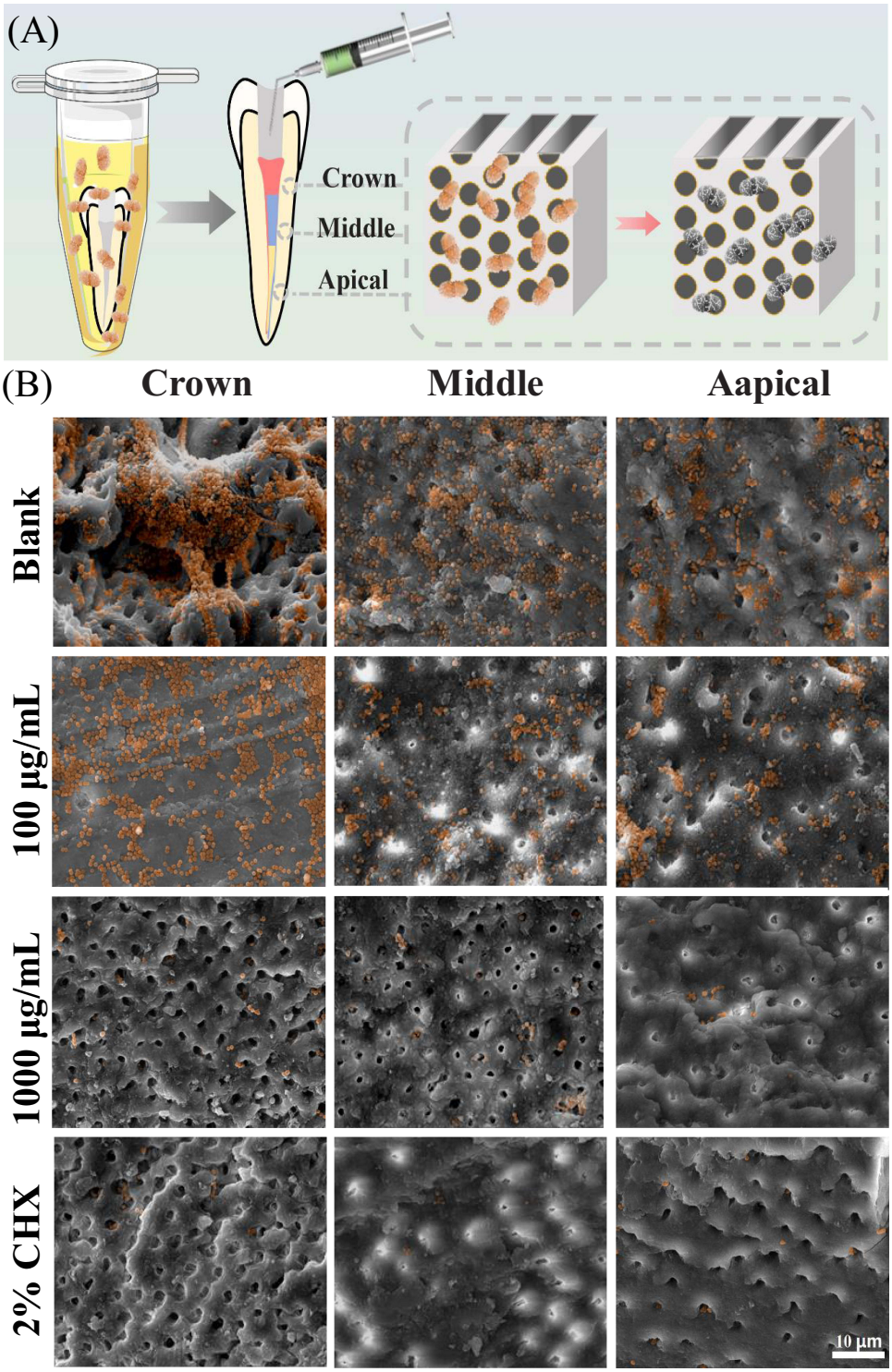

Figure 4 (**A**) Schematic diagram of the interaction between PL-CQDs and biofilms on the isolated teeth. (**B**) SEM images of the biofilms on the isolated teeth treated with PL-CQDs and 2% CHX.

Hemocompatibility and Cytocompatibility Assay

The hemocompatibility evaluation of nanomaterials is one of the major criteria for their success in clinical applicability.[53] Notably, hemolysis could cause inflammation, thrombus, the pathogenesis of sepsis, etc.[54,55] Hemolysis tests were performed to identify the hemolysis activity of PL-CQDs using defibrinated human blood. As shown in Figure 5A,

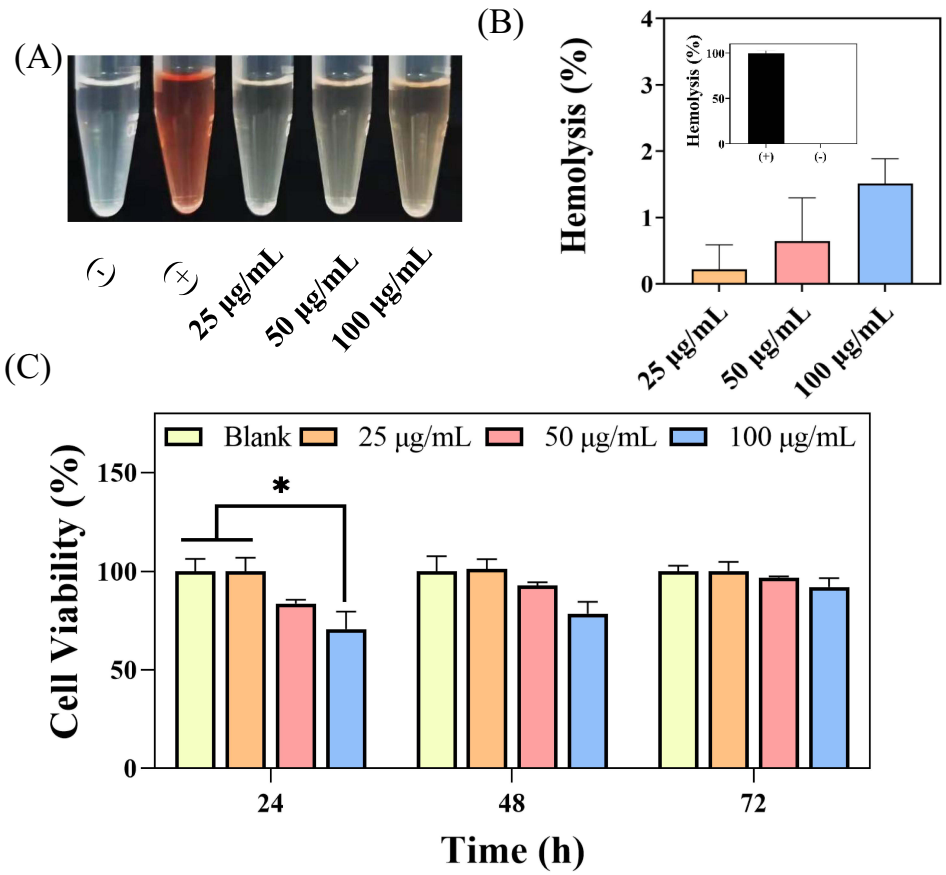

Figure 5 (**A**) Photograph of red blood cells treated with PL-CQDs. (**B**) Hemolysis rate of erythrocytes treated with PL-CQDs. Distilled water (+) and 0.9%NS (-) were used as positive and negative controls, respectively (see inset). (**C**) Cell viability of L929 after incubation with PL-CQDs.

the supernatant in all PL-CQDs samples was clear and transparent. The hemolysis rates of all PL-CQDs samples were lower than 2% (Figure 5B). This result indicates that the prepared PL-CQDs are highly selective for antibacterial activity against bacteria than against red blood cells.

We studied their cytotoxicity effect on L929 cells to evaluate PL-CQDs' cytocompatibility. Considering clinical safety and efficacy, an ideal antimicrobial agent should distinguish between bacteria and mammalian cells. At the same concentration, all bacteria were removed in a short time. At the same time, the cell survival rate exceeded 97% for 3 d of contact with the PL-CQDs, which meets the requirements of an ideal antimicrobial agent (Figure 5C). The different results of bacterial and cell killing rates after interacting with PL-CQDs may be attributed to the reasons that (i) PL-CQDs exhibit different affinities for bacteria and mammalian cells through electrostatic interactions since bacterial membrane surfaces carry more negative charges than mammalian cells. In other words, PL-CQDs preferentially interact with bacterial cells rather than mammalian cells, allowing PL-CQDs to disrupt bacterial membranes and kill micro-organisms. (ii) Relative to bacterial cells, the plasma membrane of mammalian cells contains more cholesterol to strengthen membrane integrity and reduce membrane potential, which results in a lower sensitivity to strongly positively charged PL-CQDs. Thus, the data demonstrate PL-CQDs' potential as a highly biocompatible antibacterial nanoagent.

In vivo Toxicity Test of PL-CQDs

The clearance of CDs has been widely reported previously,[56,57] in order to test the in vivo toxicity, rats were perfused with 5 mg/mL of PL-CQDs. Before execution, all rats were healthy and had no significant weight loss. After 3 and 7 d of PL-CQDs

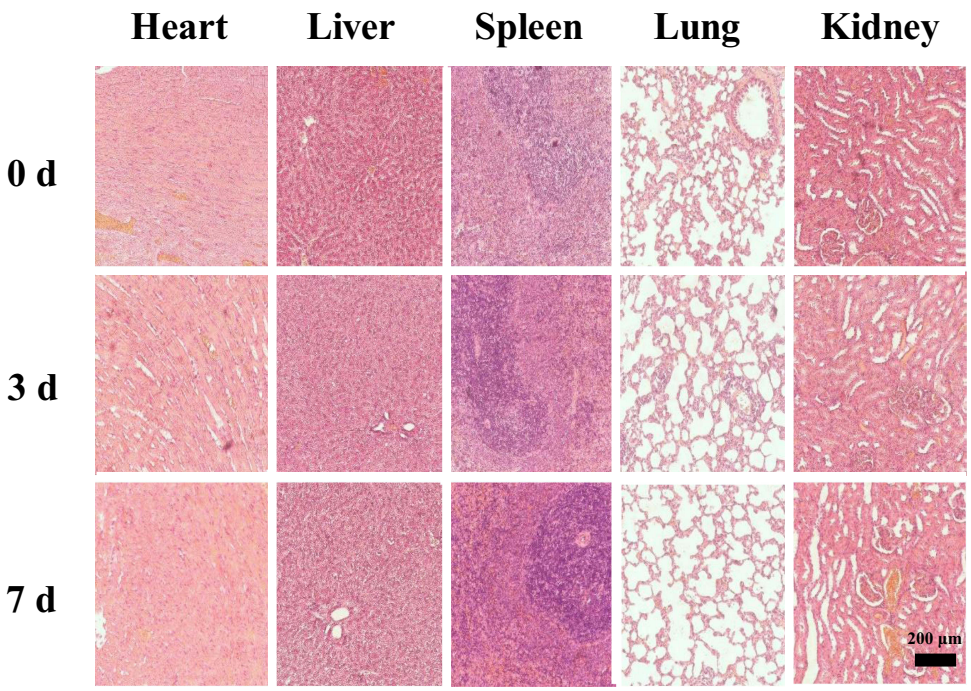

Figure 6 H&E-stained tissue slices (heart, liver, spleen, lung, and kidney) of rats perfused with PL-CQDs.

administration, the rats' hearts, liver, spleen, lungs, and kidneys were collected. It was found that there was no significant difference in appearance or color in the PL-CQDs group compared with the control group. To further verify whether PL-CQDs caused structural damage or inflammation, H&E-stained histological sections were examined for pathomorphological findings. As shown in Figure 6, compared with the control group treated with normal saline, the PL-CQDs group showed no significant damage to the structural integrity of the tissues and no obvious inflammatory cells. Further, the blood biochemical and hematological analyses were performed (Figure S4). All the parameters in the PL-CQDs groups appear normal compared with the control group and within the normal ranges. These results are in agreement with previous reports that CQDs mostly exhibit low toxicity of nanomaterials in single-dose experiments.[58,59] This suggests that PL-CQDs should be promising antimicrobial agents with negligible toxicity in vivo.

Conclusions

In summary, PL-CQDs prepared by a facile one-pot pyrolytic method displayed enhanced eradication of *E. faecalis* and related biofilm for managing persistent endodontic infections. The developed PL-CQDs (100 μg/mL) eliminated all *E. faecalis* and damaged their membrane in 5 min owing to their ultra-small size, high positive charge, and active ROS formation ability. Importantly, the fabricated PL-CQDs significantly disrupt the dense biofilm matrix to achieve full-layer killing against mature *E. faecalis* biofilms in the isolated teeth model. Additionally, biocompatibility tests showed that PL-CQDs possessed satisfactory cytocompatibility and hemocompatibility in vitro and good biosafety in vivo. Therefore, PL-CQDs provide a new strategy for eradicating bacteria associated with PEIs and have potential practical application as an ideal root canal disinfection material.

Acknowledgments

The authors are very grateful for the financial support of the Young Taishan Scholars Program of Shandong Province (Grant No. tsqn202306272), National Key Research and Development Project of China (Grant No. 2023YFFO715101), Traditional Chinese Medicine Science and Technology Project of Shandong province (Grant No. 2021Q069), the Leading Project of Science and Technology of Yantai Development Zone (Grant No. 2021RC016), and Opening Project of Hubei Key Laboratory of Biomass Fibers and Eco-Dyeing & Finishing (Grant No. STRZ202322), as well as the Qingdao Key Health

Discipline Development Fund(Grant No. 2022-2024) and Qingdao Clinical Research Center for Oral Diseases (Grant No. 22-3-7-lczx-7-nsh).

Disclosure

The authors declare no competing financial interest.

References

1. Hancock HH, Sigurdsson A, Trope M, Moiseiwitsch J. Bacteria isolated after unsuccessful endodontic treatment in a North American population. *Oral Surg Oral Med Oral Pathol Oral Radiol Endod*. 2001;91(5):579–586. doi:10.1067/moe.2001.113587
2. Sjögren U, Figdor D, Persson S, Sundqvist G. Influence of infection at the time of root filling on the outcome of endodontic treatment of teeth with apical periodontitis. *Int Endodontic J*. 1997;30(5):297–306. doi:10.1111/j.1365-2591.1997.tb00714.x
3. Stuart C, Schwartz S, Beeson T, Owatz C. Enterococcus faecalis: its role in root canal treatment failure and current concepts in retreatment. *J endodontics*. 2006;32(2):93–98. doi:10.1016/j.joen.2005.10.049
4. Chávez de Paz LE, Dahlén G, Molander A, Möller Å, Bergenholtz G. Bacteria recovered from teeth with apical periodontitis after antimicrobial endodontic treatment. *Int Endodontic J*. 2003;36(7):500–508. doi:10.1046/j.1365-2591.2003.00686.x
5. Jaju S, Jaju PP. Newer root canal irrigants in horizon: a review. *Int J Dent*. 2011;2011:9. doi:10.1155/2011/851359
6. Sedgley CM, Lennan SL, Appelbe OK. Survival of Enterococcus faecalis in root canals ex vivo. *Int Endodontic J*. 2005;38(10):735–742. doi:10.1111/j.1365-2591.2005.01009.x
7. Molander A, Reit C, Dahlén G, Kvist T. Microbiological status of root-filled teeth with apical periodontitis. *Int Endodontic J*. 1998;31(1):1–7. doi:10.1046/j.1365-2591.1998.t01-1-00111.x
8. Sundaram D, Narayanan RK, Vadakkepurayil K. A comparative evaluation on antimicrobial effect of honey, neem leaf extract and sodium hypochlorite as intracanal irrigant: an ex-vivo study. *J Clin Diagn Res*. 2016;10(8):ZC88–ZC91. doi:10.7860/JCDR/2016/19268.8311
9. Scheibler E, Garcia MCR, Medina da Silva R, Figueiredo MA, Salum FG, Cherubini K. Use of nystatin and chlorhexidine in oral medicine: properties, indications and pitfalls with focus on geriatric patients. *Gerodontology*. 2017;34(3):291–298. doi:10.1111/ger.12278
10. Siqueira JF, Lopes HP. Mechanisms of antimicrobial activity of calcium hydroxide: a critical review. *Int Endodontic J*. 1999;32(5):361–369. doi:10.1046/j.1365-2591.1999.00275.x
11. Siqueira JF, de Uzeda M. Disinfection by calcium hydroxide pastes of dentinal tubules infected with two obligate and one facultative anaerobic bacteria. *J endodontics*. 1996;22(12):674–676. doi:10.1016/S0099-2399(96)80062-8
12. Wang Y. Antibiotic-Free Antibacterial Strategies Enabled by Nanomaterials: progress and Perspectives. *Adv. Mater.* 2020;32(18):1–21. doi:10.1002/adma.201904106
13. Guo L, Wang H, Wang Y, Liu F, Feng L. Organic Polymer Nanoparticles with Primary Ammonium Salt as Potent Antibacterial Nanomaterials. *ACS Appl. Mater. Interfaces*. 2020;12(19):21254–21262. doi:10.1021/acsami.9b19921
14. Su L, Li Y, Liu Y. Recent Advances and Future Prospects on Adaptive Biomaterials for Antimicrobial Applications. *Macromol biosci*. 2019;19(12). doi:10.1002/mabi.201900289
15. Kishen A, Shi Z, Shrestha A, Neoh KG. An Investigation on the Antibacterial and Antibiofilm Efficacy of Cationic Nanoparticulates for Root Canal Disinfection. *J endodontics*. 2008;34(12):1515–1520. doi:10.1016/j.joen.2008.08.035
16. Wu D, Fan W, Kishen A, Gutmann JL, Fan B. Evaluation of the antibacterial efficacy of silver nanoparticles against Enterococcus faecalis biofilm. *J endodontics*. 2014;40(2):285–290. doi:10.1016/j.joen.2013.08.022
17. Wang H, Yu D, Fang J. Renal-Clearable Porphyrinic Metal-Organic Framework Nanodots for Enhanced Photodynamic Therapy. *ACS Nano*. 2019;13(8):9206–9217. doi:10.1021/acsnano.9b03531
18. Soo Choi H, Liu W, Misra P. Renal clearance of quantum dots. *Nature Biotechnol*. 2007;25(10):1165–1170. doi:10.1038/nbt1340
19. Yang J, Gao G, Zhang X. Ultrasmall and photostable nanotheranostic agents based on carbon quantum dots passivated with polyamine-containing organosilane molecules. *Nanoscale*. 2017;9(40):15441–15452. doi:10.1039/c7nr05613c
20. Hua X-W, Bao Y-W, Chen Z, Wu F-G. Carbon quantum dots with intrinsic mitochondrial targeting ability for mitochondria-based theranostics. *Nanoscale*. 2017;9(30):10948–10960. doi:10.1039/c7nr03658b
21. Hua X-W, Bao Y-W, Wu F-G. Fluorescent Carbon Quantum Dots with Intrinsic Nucleolus-Targeting Capability for Nucleolus Imaging and Enhanced Cytosolic and Nuclear Drug Delivery. *ACS Appl. Mater. Interfaces*. 2018;10(13):10664–10677. doi:10.1021/acsami.7b19549
22. Hutton GAM, Martindale BCM, Reisner E. Carbon dots as photosensitisers for solar-driven catalysis. *Chem. Soc. Rev.* 2017;46(20):6111–6123. doi:10.1039/c7cs00235a
23. Zhang X, Wang J, Liu J, Wu J, Chen H, Bi H. Design and preparation of a ternary composite of graphene oxide/carbon dots/polypyrrole for supercapacitor application: importance and unique role of carbon dots. *Carbon*. 2017;115:134–146. doi:10.1016/j.carbon.2017.01.005
24. Nan Z, Hao C, Zhang X, Liu H, Sun R. Carbon quantum dots (CQDs) modified ZnO/CdS nanoparticles based fluorescence sensor for highly selective and sensitive detection of Fe(III). *Spectrochimica Acta Part A*. 2020;228(Iii):117717. doi:10.1016/j.saa.2019.117717
25. Wang Y, Hu A. Carbon quantum dots: synthesis, properties and applications. *J Mater Chem C*. 2014;2(34):6921–6939. doi:10.1039/c4tc00988f
26. Ge J, Lan M, Zhou B. A graphene quantum dot photodynamic therapy agent with high singlet oxygen generation. *Nat Commun*. 2014;5. doi:10.1038/ncomms5596
27. Alexiades-Armenakas M. Laser-mediated photodynamic therapy. *Clin Dermatol*. 2006;24(1):16–25. doi:10.1016/j.clindermatol.2005.10.027
28. Igney FH, Krammer PH. Death and anti-death: tumour resistance to apoptosis. *Nat Rev Cancer*. 2002;2(4):277–288. doi:10.1038/nrc776
29. Abu Rabe DI, Al Awak MM, Yang F. The dominant role of surface functionalization in carbon dots' photo-activated antibacterial activity. *Int j Nanomed*. 2019;14:2655–2665. doi:10.2147/IJN.S200493
30. Meziani MJ, Dong X, Zhu L. Visible-Light-Activated Bactericidal Functions of Carbon "quantum" Dots. *ACS Appl. Mater. Interfaces*. 2016;8(17):10761–10766. doi:10.1021/acsami.6b01765

31. Li Y-J, Harroun SG, Su Y-C. Synthesis of Self-Assembled Spermidine-Carbon Quantum Dots Effective against Multidrug-Resistant Bacteria. *Adv. Healthcare Mater.* 2016;5(19):2545–2554. doi:10.1002/adhm.201600297
32. Yang J, Gao G, Zhang X, Ma Y-H, Chen X, Wu F-G. One-step synthesized carbon dots with bacterial contact-enhanced fluorescence emission property: fast Gram-type identification and selective Gram-positive bacterial inactivation. *Carbon*. 2019;146:827–839. doi:10.1016/j.carbon.2019.02.040
33. Hou P, Yang T, Liu H, Li YF, Huang CZ. An active structure preservation method for developing functional graphitic carbon dots as an effective antibacterial agent and a sensitive pH and Al(iii) nanosensor. *Nanoscale*. 2017;9(44):17334–17341. doi:10.1039/c7nr05539k
34. Yang J, Zhang X, Ma Y-H. Carbon Dot-Based Platform for Simultaneous Bacterial Distinguishment and Antibacterial Applications. *ACS Appl. Mater. Interfaces*. 2016;8(47):32170–32181. doi:10.1021/acsami.6b10398
35. Ge J, Lan M, Zhou B. Rapid and Superior Bacteria Killing of Carbon Quantum Dots/ZnO Decorated Injectable Folic Acid-Conjugated PDA Hydrogel through Dual-Light Triggered ROS and Membrane Permeability. *Small*. 2019;15(22):1–15. doi:10.1002/smll.201900322
36. Kováčová M, Marković ZM, Humpolíček P. Carbon Quantum Dots Modified Polyurethane Nanocomposite as Effective Photocatalytic and Antibacterial Agents. *ACS Biomater. Sci. Eng.* 2018;4(12):3983–3993. doi:10.1021/acsbiomaterials.8b00582
37. Dong X, Awak MA, Tomlinson N, Antibacterial effects of carbon dots in combination with other antimicrobial reagents. *PLoS One*. 2017;12(9):1–16. doi:10.1371/journal.pone.0185324
38. Yan Y, Kuang W, Shi L. Carbon quantum dot-decorated TiO2 for fast and sustainable antibacterial properties under visible-light. *Journal of Alloys and Compounds*. 2019;777:234–243. doi:10.1016/j.jallcom.2018.10.191
39. Sidhu JS, Pandiyan T, Kaur N, Singh N. The Photochemical Degradation of Bacterial Cell Wall Using Penicillin-Based Carbon Dots: weapons Against Multi-Drug Resistant (MDR) Strains. *ChemistrySelect*. 2017;2(29):9277–9283. doi:10.1002/slct.201701810
40. Jijie R, Barras A, Bouckaert J, Dumitrascu N, Szunerits S, Boukherroub R. Enhanced antibacterial activity of carbon dots functionalized with ampicillin combined with visible light triggered photodynamic effects. *Colloids Surf. B*. 2018;170:347–354. doi:10.1016/j.colsurfb.2018.06.040
41. Zhang J, Liu X, Wang X. Carbon dots-decorated Na 2 W 4 O 13 composite with WO 3 for highly efficient photocatalytic antibacterial activity. *J Hazard Mater*. 2018;359(February):1–8. doi:10.1016/j.jhazmat.2018.06.072
42. Al Awak MM. Correlation of carbon dots' light-activated antimicrobial activities and fluorescence quantum yield. *RSC Adv.* 2017;7(48):30177–30184. doi:10.1039/c7ra05397e
43. Mosquera J, García I, Liz-Marzán LM. Cellular Uptake of Nanoparticles versus Small Molecules: a Matter of Size. *Acc. Chem. Res.* 2018;51(9):2305–2313. doi:10.1021/acs.accounts.8b00292
44. Bao L, Liu C, Zhang Z-L, Pang D-W. Photoluminescence-tunable carbon nanodots: surface-state energy-gap tuning. *Adv. Mater.* 2015;27(10):1663–1667. doi:10.1002/adma.201405070
45. Sun B, Wu F, Zhang Q. Insight into the effect of particle size distribution differences on the antibacterial activity of carbon dots. *J Colloid Interface Sci*. 2021;584:505–519. doi:10.1016/j.jcis.2020.10.015
46. Dong Y, Wang R, Li H. Polyamine-functionalized carbon quantum dots for chemical sensing. *Carbon*. 2012;50(8):2810–2815. doi:10.1016/j.carbon.2012.02.046
47. Helander IM, Nurmiaho-Lassila E-L, Ahvenainen R, Rhoades J, Roller S. Chitosan disrupts the barrier properties of the outer membrane of Gram-negative bacteria. *Int J Food Microbiol*. 2001;71(2–3):235–244. doi:10.1016/S0168-1605(01)00609-2
48. Wu M, Wang Y, Wu W. Preparation of functionalized water-soluble photoluminescent carbon quantum dots from petroleum coke. *Carbon*. 2014;78:480–489. doi:10.1016/j.carbon.2014.07.029
49. Tew GN, Scott RW, Klein ML, DeGrado WF. De novo design of antimicrobial polymers, foldamers, and small molecules: from discovery to practical applications. *Acc. Chem. Res.* 2010;43(1):30–39. doi:10.1021/ar900036b
50. Costerton JW, Stewart PS, Greenberg EP. Bacterial biofilms: a common cause of persistent infections. *Science*. 1999;284(5418):1318–1322. doi:10.1126/science.284.5418.1318
51. Nair PNR. On the causes of persistent apical periodontitis: a review. *Int Endodontic J*. 2006;39(4):249–281. doi:10.1111/j.1365-2591.2006.01099.x
52. Lim Z, Cheng JL, Lim TW. Light activated disinfection: an alternative endodontic disinfection strategy. *Australian Dental J*. 2009;54(2):108–114. doi:10.1111/j.1834-7819.2009.01102.x
53. Maitz MF, Sperling C, Wongpinyochit T. Biocompatibility assessment of silk nanoparticles: hemocompatibility and internalization by human blood cells. *Nanomed Nanotechnol Biol Med*. 2017;13(8):2633–2642. doi:10.1016/j.nano.2017.07.012
54. Van Avondt K, Nur E, Zeerleder S. Mechanisms of haemolysis-induced kidney injury. *Nat Rev Nephrol*. 2019;15(11):671–692. doi:10.1038/s41581-019-0181-0
55. Bartoli CR, Zhang D, Kang J. Clinical and In Vitro Evidence That Subclinical Hemolysis Contributes to LVAD Thrombosis. *Ann Thorac Surg*. 2018;105(3):807–814. doi:10.1016/j.athoracsur.2017.05.060
56. Ramana LN, Dinh LNM, Agarwal V. Influence of surface charge of graphene quantum dots on their uptake and clearance in melanoma cells. *Nanoscale Adv*. 2021;3(12):3513–3521. doi:10.1039/d0na00935k
57. Fischer H, Liu L, Pang K, Chan W. Pharmacokinetics of nanoscale quantum dots: in vivo distribution, sequestration, and clearance in the rat. *Adv. Funct. Mater.* 2006;16(10):1299–1305. doi:10.1002/adfm.200500529
58. Tao H, Yang K, Ma Z. In vivo NIR fluorescence imaging, biodistribution, and toxicology of photoluminescent carbon dots produced from carbon nanotubes and graphite. *Small*. 2012;8(2):281–290. doi:10.1002/smll.201101706
59. Huang X, Zhang F, Zhu L. Effect of injection routes on the biodistribution, clearance, and tumor uptake of carbon dots. *ACS Nano*. 2013;7(7):5684–5693. doi:10.1021/nn401911k